

Fluorescence tumor imaging by i.v. administered indocyanine green in a mouse model of colitis-associated colon cancer

Rei Nagahara¹ | Nobuhiko Onda^{1,2} | Susumu Yamashita² | Miho Kojima^{1,2} |
Mari Inohana¹ | Ayumi Eguchi¹ | Misato Nakamura¹ | Shinya Matsumoto² |
Toshinori Yoshida¹ | Makoto Shibutani^{1,3} 

¹Division of Animal Life Science, Laboratory of Veterinary Pathology, Institute of Agriculture, Tokyo University of Agriculture and Technology, Tokyo, Japan

²Evaluation Technology Department 1, R&D Group, Olympus Corporation, Tokyo, Japan

³Institute of Global Innovation Research, Tokyo University of Agriculture and Technology, Tokyo, Japan

Correspondence

Makoto Shibutani, Laboratory of Veterinary Pathology, Division of Animal Life Science, Institute of Agriculture, Tokyo University of Agriculture and Technology, Tokyo, Japan.
Email: mshibuta@cc.tuat.ac.jp

Funding information

This research was supported by Olympus Corporation and by a Research Fund from the Institute of Global Innovation Research, Tokyo University of Agriculture and Technology.

Fluorescence tumor imaging using exogenous fluorescent tumor-targeting agents has potential to improve early tumor detection. The fluorescent contrast agent indocyanine green (ICG) is used in medical diagnostics. The aim of the present study is to investigate the tumor imaging capability and the imaging mechanism of i.v. administered ICG in a mouse model of colitis-associated colon cancer. To do this, an azoxymethane/dextran sodium sulfate-induced colon cancer mouse model was used. Ex vivo imaging experiments were carried out 1 hour after i.v. injection of ICG. The ICG fluorescence was observed in the colon tumor tissues, with sufficient tumor to normal tissue ratio, correlating with tumor malignancy. In the tumor tissues, ICG fluorescence was localized in the vascular interstitial tissue. Immunofluorescence microscopy revealed that tumor cells formed tight junctions normally, suggesting an inability of tumor cellular uptake of ICG. In contrast, tumor tissues increased the CD31-immunoreactive endothelial cell area, and accumulated stromal cells immunoreactive for COX-2 and tumor cell population immunoreactive for inducible nitric oxide synthase. In vivo vascular permeability assay revealed that prostaglandin E₂ promoted the endothelial cell permeability of ICG. In conclusion, our data indicated that fluorescence contrast-enhanced imaging following i.v. administered ICG can be applied to the detection of colon tumors in a mouse colitis-associated colon cancer model. The tumor tissue preference of ICG in the present model can be attributed to the enhanced vascular leakage of ICG involving inflammatory mediators, such as COX-2 and inducible nitric oxide synthase, in conjunction with increased tumor vascularity.

KEYWORDS

colitis-associated colon cancer, fluorescence imaging, indocyanine green, tumor malignancy, vascular permeability

Abbreviations: AOM, azoxymethane; CCD, charge-coupled device; DSS, dextran sodium sulfate; HO-1, heme oxygenase-1; ICG, indocyanine green; iNOS, inducible nitric oxide synthase; LPS, lipopolysaccharide; NTCP, sodium-taurocholate co-transporting polypeptide; PGE₂, prostaglandin E₂; TL488, *Lycopersicon esculentum* (tomato) lectin conjugated with DyLight 488.

This is an open access article under the terms of the Creative Commons Attribution-NonCommercial-NoDerivs License, which permits use and distribution in any medium, provided the original work is properly cited, the use is non-commercial and no modifications or adaptations are made.

© 2018 The Authors. *Cancer Science* published by John Wiley & Sons Australia, Ltd on behalf of Japanese Cancer Association.

1 | INTRODUCTION

Inflammatory bowel disease, such as Crohn's disease or ulcerative colitis, is a risk factor for the development of colitis-associated colorectal cancer.¹⁻³ It is difficult to detect colitis-associated colorectal cancer using white-light colonoscopy because of the background mucosal changes associated with long-term colitis and morphological diversity of the cancer.⁴ Therefore, for screening colonoscopy to detect dysplasia or early stage cancer, four random biopsies every 10 cm of the whole colorectal tissue using white-light endoscopy has traditionally been recommended.⁴ However, this approach is quite cumbersome and time consuming. Therefore, the development of detection techniques that provide biological information with sufficient sensitivity and specificity is necessary to improve the current situation.

Fluorescence tumor imaging using exogenous fluorescent tumor-targeting agents has been investigated for applications in endoscopy.⁵⁻⁷ In this technique, neoplastic lesions are visually enhanced with specific biomarkers targeted by the fluorescent agents. The advantages of fluorescence tumor imaging include its high specificity and sensitivity, real-time video frame-rate imaging, relatively low cost, portability, and the absence of radiation exposure.^{8,9} It may, therefore, be a valuable method in early cancer detection. However, despite the variety of tumor imaging agents developed thus far, many of those intended for use in humans are still in preclinical or early phase clinical trials.⁶

Indocyanine green is a fluorescent contrast agent approved for clinical applications in the USA and some European and Asian countries, including Japan. Because i.v. administered ICG is excreted exclusively by the liver, it has been used for decades to assess hepatic function in humans and has an excellent safety profile.¹⁰ Recently, tumor accumulation of ICG has been reported in a variety of tumor types, including tumors of the liver,^{11,12} breast,¹³ head and neck,¹⁴ and lungs¹⁵ in humans. Detection of tumor metastatic lesions using ICG has also been reported in ovaries¹⁶ and colon.¹⁷⁻²⁰ However, the mechanism allowing tumor detection by ICG is poorly understood.

Currently, there are three potential mechanisms of ICG-based tumor imaging. In hepatic tumors, ICG positivity is partly correlated with influx transporters, organic anion transporting polypeptide 1B3 and Ntcp,^{21,22} both of which are normally expressed in hepatocytes and mediate the cellular uptake of ICG *in vitro*.²³ In experimental tumor models of the colon, endocytosis associated with tight junction disruption of the epithelial cells has been shown to increase ICG uptake capability.^{24,25} In other cases, ICG-based tumor imaging is thought to be caused by the enhanced permeability and retention effect of the nano-sized ICG-plasma protein complex.²⁶ Indocyanine green fluorescence signal intensity in the tumor tissues correlates with microvascular density,²⁷ which is one of the parameters affecting the enhanced permeability and retention effect. Revealing the tumor imaging mechanism of ICG supports the precise clinical usage of ICG in tumor detection.

The aim of this study is to investigate the tumor imaging capability and the imaging mechanism of i.v. administered ICG in a mouse

model of colitis-associated colon cancer. To do this, we examined the imaging capability of ICG using *ex vivo* wide-field imaging in an AOM/DSS-induced colon carcinogenesis model. We further investigated the mechanism underlying tumor tissue uptake of ICG using *ex vivo* microscopic imaging, immunofluorescence analysis, and cultured cell experiments.

2 | MATERIALS AND METHODS

2.1 | Fluorescent agents

Pharmaceutical grade ICG was purchased from Daiichi-Sankyo (Diagnogreen; Tokyo, Japan). Blood vessels were visualized using TL488 (Vector Laboratories, Burlingame, CA, USA).

2.2 | Fluorescence imaging systems

The basic specifications of fluorescence imaging systems has been reported previously.²⁴ Briefly, macroscopic images were captured using a fluorescence reflectance imaging system (OV100; Olympus, Tokyo, Japan) equipped with a 150 W xenon light source and a color digital CCD camera (DP71; Olympus). Excitation and emission filters for ICG fluorescence imaging were 730 ± 22.5-nm band-pass and 770-nm long-pass filter, respectively. High-power view was observed using a multi-wavelength laser scanning microscope (IV100; Olympus) equipped with a 748-nm diode laser with 17 mW power output and a photomultiplier tube. The emission filter to detect ICG fluorescence was a 779-nm long-pass filter. Tissue sections were scanned using a fluorescence virtual microscopy system (VS120-FL; Olympus) equipped with a 200 W mercury light source (X-Cite exacte; Excelitas Technologies, Waltham, MA, USA) and a monochrome digital CCD camera (ORCA-R2; Hamamatsu Photonics, Hamamatsu, Japan). Excitation and emission filters for ICG fluorescence were 708 ± 37.5-nm band-pass and 809 ± 40.5-nm band-pass filter, respectively. Fluorescence images are shown in grayscale or pseudo-colors.

2.3 | Experimental tumor model

The AOM/DSS-induced colitis-associated colon cancer mouse model was constructed according to the methods described previously,²⁸⁻³⁰ with some modifications. The 38 female ICR mice (4 weeks old) used in this study were purchased from Japan SLC (Shizuoka, Tokyo). They were fed MF (Oriental Yeast, Tokyo, Japan) as a basal diet and provided with water *ad libitum* throughout the experimental period. Starting at 5 weeks of age, the mice received a single i.p. injection of AOM (10 mg/kg body weight; Sigma-Aldrich, St. Louis, MO, USA). One week after the AOM injections, recurrent colitis was induced by administration of 5 w/v% DSS (MP Biochemicals, Santa Ana, CA, USA) in drinking water for 1 week. The mice that showed severe weight loss or serious hematochezia during the 1 week of DSS treatment had their DSS discontinued immediately. For *in vivo* vascular permeability assay, four female BALB/c nude mice (7 weeks old)

were purchased from Japan SLC. They received CA-1 (Nihon CLEA, Tokyo, Japan) as a basal diet and tap water ad libitum throughout the experimental period. All animal experiments were undertaken in

accordance with the guidelines for animal experimentation of the Faculty of Agriculture, Tokyo University of Agriculture and Technology (Tokyo, Japan).

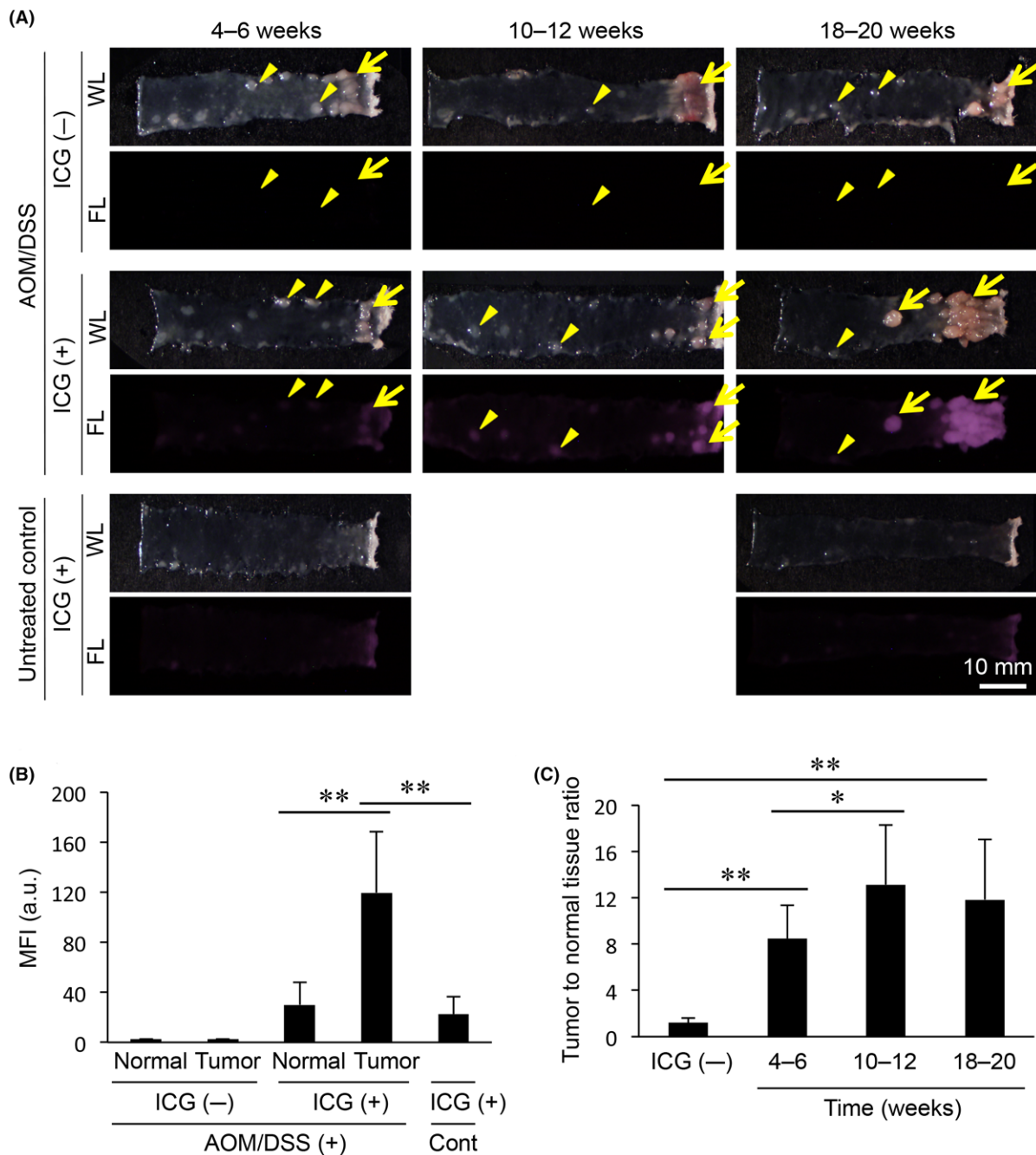


FIGURE 1 Ex vivo imaging of mouse colon tumor tissues after i.v. administration of indocyanine green (ICG). Colon tissues of azoxymethane (AOM)/dextran sodium sulfate (DSS)-treated mice with/without ICG injection or untreated mice with ICG injection were subjected to observation 1 h after i.v. administration of ICG at 4-6, 10-12, and 18-20 weeks after AOM initiation. (A) White light (WL) images or fluorescence (FL) images (magenta) in each time period. Arrows and arrowheads indicate tumor tissues and lymphoid follicles, respectively. (B) Mean fluorescence intensity (MFI) of ICG in colon tissues in the time period of 18-20 weeks after AOM initiation. Treatment groups: $n = 6$ for both non-tumor and tumor tissues in AOM/DSS⁺-ICG⁻; $n = 47$ for non-tumor tissues; $n = 40$ for tumor tissues in AOM/DSS⁺-ICG⁺; and $n = 14$ for normal tissues control (Cont)-ICG⁺. Values represent mean + SD. $^{***}P < .01$ (Tukey-Kramer's test or Steel-Dwass test). (C) Tumor to normal tissue ratio of MFI of ICG in each time period: $n = 24$ for ICG⁻; $n = 15$ for 4-6 weeks; $n = 23$ for 10-12 weeks; and $n = 42$ for 18-20 weeks. Values represent mean + SD. $^{*}P < .05$; $^{***}P < .01$ (Tukey-Kramer's test or Steel-Dwass test)

2.4 | Ex vivo imaging

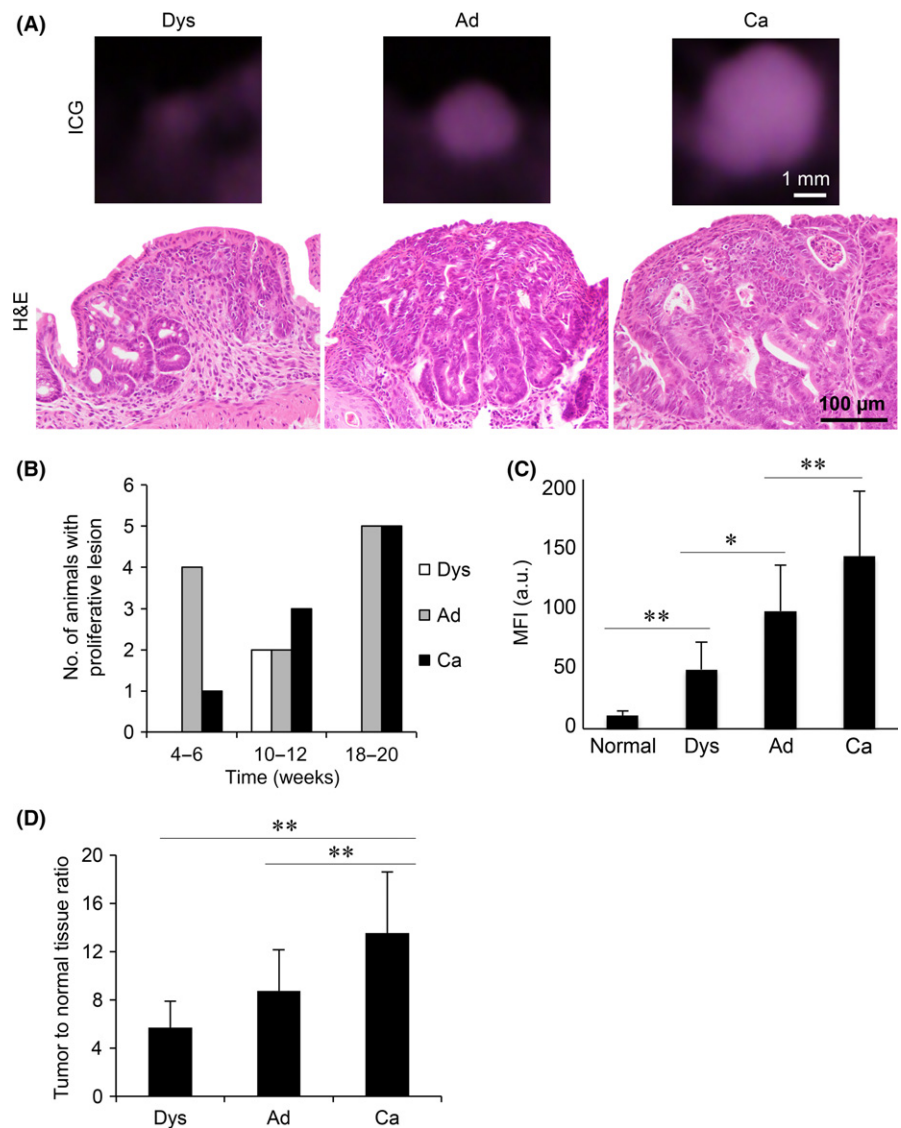
Imaging experiments were carried out 4–6, 10–12, and 18–20 weeks after injection of AOM ($n = 10$ – 11 for each time period). The AOM/DSS-treated mice ($n = 5$ for 4–6 weeks, $n = 6$ for 10–12 weeks, and $n = 9$ for 18–20 weeks) were i.v. injected with 100 μL (7.5 mg/kg) ICG²⁴ and left untreated for 1 hour. The blood circulation time of ICG was determined based on the results of preliminary experiments of ex vivo colon tumor imaging at different exposure time points ($n = 1$ each for 30 minutes and 6 hours at the time period of 4–6 weeks; Figure S1). The AOM/DSS-treated mice without ICG injection were also prepared ($n = 3$ for 4–6 weeks and 10–12 weeks, and $n = 1$ for 18–20 weeks). The AOM/DSS-untreated control mice were injected with ICG ($n = 3$ for 4–6 and $n = 3$ for 18–20 weeks). In these animals, TL488 was i.v. injected at 100 $\mu\text{g}/100 \mu\text{L}$ per mouse 10 minutes before they were killed by exsanguination under isoflurane anesthesia. The excised colon tissues were cut to reveal the intestinal mucosa, washed with PBS (pH 7.4), and then subjected to ex vivo imaging. As a control, colon tissues from AOM/DSS-treated

mice without ICG administration or normal mice with ICG administration were used. A preliminary experiment with an ICG enema was also undertaken, as previously reported.²⁵ The AOM/DSS-treated mice ($n = 1$ each for 4–6 and 10–12 weeks) were given 500 μL ICG at 30 $\mu\text{g}/\text{mL}$ by enema and then subjected to imaging analysis as described above.

2.5 | Histology and immunofluorescence

In all animals, the excised colon tissues used in the histopathological examination were fixed overnight in phosphate-buffered 10% formalin (pH 7.4). Paraffin-embedded tissue sections stained with H&E were used to diagnose the proliferative lesions in the mouse colon. The proliferative lesions were histopathologically classified as dysplasia, adenoma, and adenocarcinoma.^{30,31} Immunofluorescence was carried out using methanol-fixed snap-frozen sections of colon tissues obtained from the mice 18–20 weeks after their i.p. injection of AOM. The sections were incubated with primary antibodies (Table S1) overnight at 4°C, and then with species-appropriate

FIGURE 2 Ex vivo indocyanine green (ICG) fluorescence imaging of mouse colon tumor tissues during tumor development. Colon tissues of azoxymethane (AOM)/dextran sodium sulfate (DSS)-treated mice with ICG injection were subjected to observation 1 h after i.v. injection of ICG at 4–6, 10–12, and 18–20 weeks after AOM initiation. (A) Representative ICG fluorescence images of colon dysplasia (Dys), adenoma (Ad), and adenocarcinoma (Ca) tissues and corresponding H&E stained images (magnification, $\times 200$). (B) Number of animals bearing each type of proliferative lesion in AOM/DSS-treated mice that received i.v. injection of ICG with 1 h of circulation time in each time period. (C) Mean fluorescence intensity (MFI) of ICG in each type of tissue: $n = 51$ for normal tissues; $n = 6$ for Dys; $n = 31$ for Ad; and $n = 48$ for Ca. Values represent mean + SD. $*P < .05$; $**P < .01$ (Tukey-Kramer's test or Steel-Dwass test). (D) Tumor to normal tissue ratio of MFI of ICG in each type of proliferative lesion: $n = 6$ for Dys; $n = 31$ for Ad; and $n = 48$ for Ca. Values represent mean + SD. $**P < .01$ (Tukey-Kramer's test or Steel-Dwass test)



antibodies labeled with Alexa Fluor 488 or 594 (Thermo Fisher Scientific, Waltham, MA, USA) for 1 hour at room temperature, and counterstained with DAPI (Thermo Fisher Scientific).

2.6 | In vivo vascular permeability assay

In vivo vascular permeability was measured as reported previously,³² with some modifications. Prostaglandin E₂ (2 µg/20 µL/ear) was intradermally injected to the right ear of the normal nude mice (n = 4). As a control, the same amount of PBS was injected to the left ear. Fifteen minutes after PGE₂ injection, ICG (7.5 mg/kg body weight) was given i.v. One minute after ICG injection, macroscopic imaging using OV100 was carried out to detect vascularity of the ears. Approximately 10–12 min after ICG injection, ICG accumulation in the ear was observed by IV100. Fluorescence signals were measured using OV100 or IV100 software.

2.7 | Statistical analysis

Fluorescence images were analyzed using ImageJ software (NIH, Bethesda, MD, USA). The mean fluorescence intensity of ICG in colon tissues was measured and then the tumor to normal tissue ratio was calculated. Numerical data are presented as the mean ± SD. Numerical data of the in vivo study, consisting of more than three sample groups, were assessed using Tukey–Kramer's test after verification of homogeneity of the variances by Bartlett's test. The Steel–Dwass test was applied for heterogeneous data. Numerical data of the in vitro study, consisting of four sample groups, were analyzed using Bartlett's test for homogeneity of variance. If the variance was homogenous, numerical data were assessed using Dunnett's test. For heterogeneous data, Steel's test was applied. The matched-pair *t*-test was applied to compare ICG fluorescence signal difference between the PGE₂ injection side and PBS injection side.

3 | RESULTS

3.1 | Colon tumor detection capability of i.v. ICG in a mouse model of colitis-associated colon cancer

No colonic proliferative lesions were observed in two mice of the 10–12-observation week group, and one in the 18–20-observation week group in AOM/DSS-treated mice. All of the remaining AOM/DSS-treated mice revealed multiple proliferative lesions of various sizes in the perianal area. Ex vivo wide-field imaging revealed strong ICG fluorescence in proliferative lesions in each time period (Figure 1A, Figure S1), whereas autofluorescence was rarely observed in ICG non-administered AOM/DSS-treated mice (Figure 1A, Figure S1). In the untreated control mice injected with ICG, slight ICG fluorescence was only observed at the perianal area, reflecting the thickness of the perianal tissues. Lymphoid follicles in the colon tissues also showed moderate ICG fluorescence in ICG-administered mice (Figure 1A). Indocyanine green fluorescence signal in the

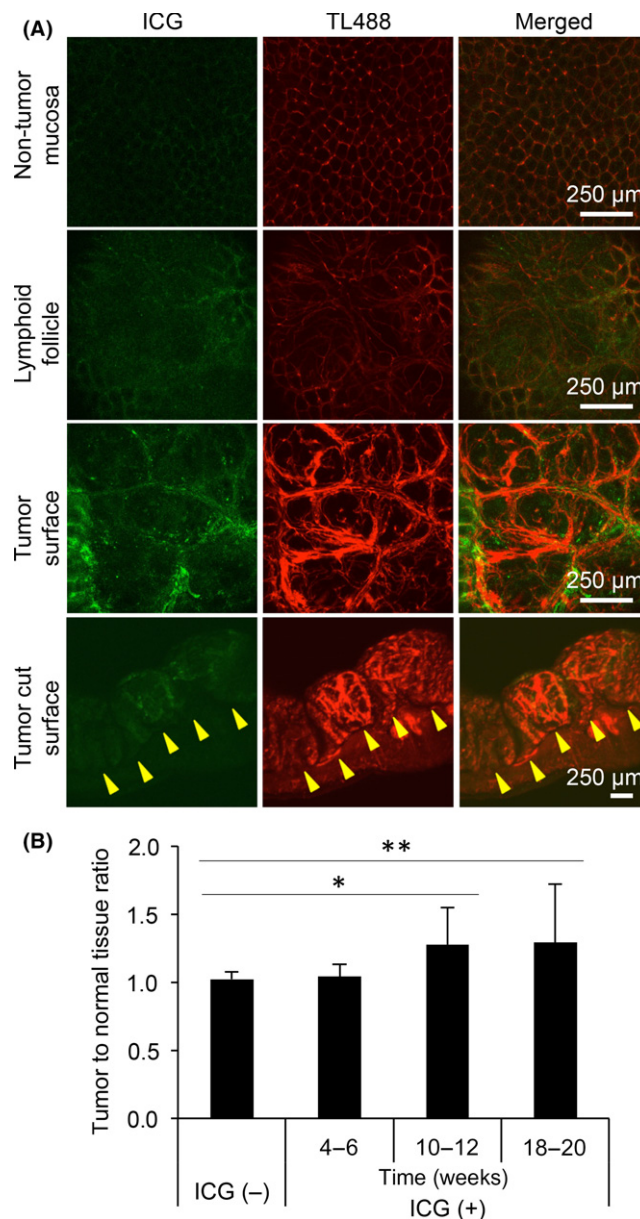


FIGURE 3 Microscopic imaging of indocyanine green (ICG) fluorescence distribution in mouse colon tumor tissues. High-power view of colon tissues in azoxymethane (AOM)/dextran sodium sulfate (DSS)-treated mice with/without ICG injection was acquired 1 h after i.v. administration of ICG at 4–6, 10–12, and 18–20 weeks after AOM initiation. (A) ICG fluorescence images (green) with *Lycopersicon esculentum* (tomato) lectin conjugated with DyLight 488 (TL488) fluorescence (red) staining blood vessels in AOM/DSS-treated mice with ICG injection in the time period of 18–20 weeks after AOM initiation. Arrowheads indicate the border of mucosal and muscle layers. (B) Tumor to normal tissue ratio of mean fluorescence intensity of ICG in high-power view of colon tumor tissues. The data of AOM/DSS-treated ICG non-administered group were shown as a sum of mice obtained from each time period (n = 1 for 4–6 weeks, n = 2 for 10–12 weeks, and n = 1 for 18–20 weeks). The sample number of tumor tissues was n = 6 for 4–6 weeks, n = 14 for 10–12 weeks, and n = 34 for 18–20 weeks, respectively. Values represent mean + SD. **P* < .05 and ***P* < .01 (Tukey–Kramer's test or Steel–Dwass test)

proliferative lesions in AOM/DSS-treated mice was significantly higher than that of colon tissues in normal mice or non-tumor tissues in AOM/DSS-treated mice (Figure 1B, Figure S1). In AOM/DSS-treated mice, the tumor to normal tissue ratio was >2 and significantly higher than that of the ICG non-administered group in each time period (Figure 1C).

3.2 | Changes in ICG fluorescence signal during tumor development

Histologically, AOM/DSS-treated mice developed multiple mucosal proliferative lesions of dysplasia, adenoma, and adenocarcinoma, all showing ICG fluorescence (Figure 2A,B). The macroscopic ICG fluorescence signal was significantly increased in the colon proliferative lesions compared with normal mucosa, accompanying significant signal increases in more advanced lesions (Figure 2C). The tumor to normal tissue ratio of ICG fluorescence was also significantly increased in more advanced lesions (Figure 2D). The ICG fluorescence data were applied to construct receiver operating characteristic curves as well as scatter plot to determine detection capability of mucosal proliferative lesions from dysplasia to adenocarcinoma in ICG fluorescence imaging (Figures S2 and S3). As a result, the sensitivity/specificity for detection of the proliferative lesions was 87.1%/89.6% for proliferative lesions (cut-off mean fluorescence intensity: 56.4 arbitrary units) and 63.8%/90.3% for differentiation of adenocarcinoma from adenoma (cut-off mean fluorescence intensity, 143.6 arbitrary units), respectively.

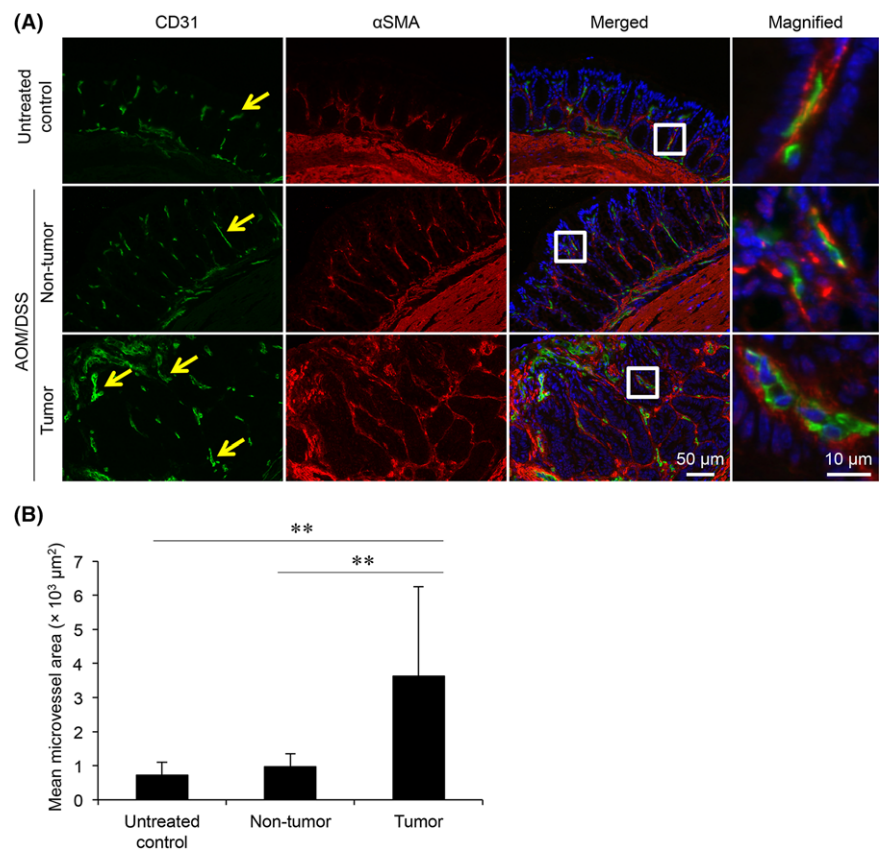
3.3 | Microscopic analysis of ICG fluorescence localization in the colon tumor tissues

Ex vivo microscopic imaging revealed that blood vessels in the tumor tissues showed distorted and thick vasculatures compared with normal mucosal blood vessels (Figure 3A). In the tumor tissues, ICG fluorescence was distributed in the stromal tissues around the blood vessels in each time period (Figure 3A, Figure S1). The ICG fluorescence was unevenly distributed in the mucosa and not in the muscle layer (Figure 3A). Indocyanine green fluorescence was not observed in the tumor parenchyma in any time period (Figures 3A, Figures S1). The tumor to normal tissue ratio of ICG fluorescence in mice 10-12 or 18-20 weeks after injection of AOM was significantly higher than that in the ICG non-administered group (Figure 3B).

3.4 | Vascular component analysis in colon tumor tissues

The area of CD31⁺ endothelial cells in the tumor tissues was larger and thicker than that of normal colon tissues (Figure 4A). CD31⁺ endothelial cells covered with/without α -smooth muscle actin-positive pericytes were observed in both normal colon tissues from untreated mice or AOM/DSS-treated mice and tumor tissues from AOM/DSS-treated mice (Figure 4A). The CD31⁺ area in the tumor tissues was significantly increased compared with that of normal colon tissues from untreated mice or AOM/DSS-treated mice

FIGURE 4 Immunofluorescence imaging of blood vessel components in the colon tumor tissues. Immunofluorescence of CD31 (green) and α -smooth muscle actin (α SMA) (red) with nuclear staining (blue) was carried out using the colon tissue sections obtained from azoxymethane (AOM)/dextran sodium sulfate (DSS)-treated mice or untreated mice at 18-20 weeks after AOM initiation. (A) Immunofluorescence images of CD31 and α SMA. Immunofluorescence images as shown in the boxed areas indicate the field-of-view of the magnified images. Arrows indicate CD31⁺ endothelial cells. (B) Mean microvessel area showing CD31⁺ endothelial cell-occupied area in the field-of-view ($1.82 \times 10^4 \mu\text{m}^2$; $n = 12$ for normal tissues from non-treated mice, $n = 14$ for non-tumor tissues, and $n = 36$ for tumor tissues from AOM/DSS-treated mice). Values represent mean + SD. ** $P < .01$ (Tukey-Kramer's test or Steel-Dwass test)



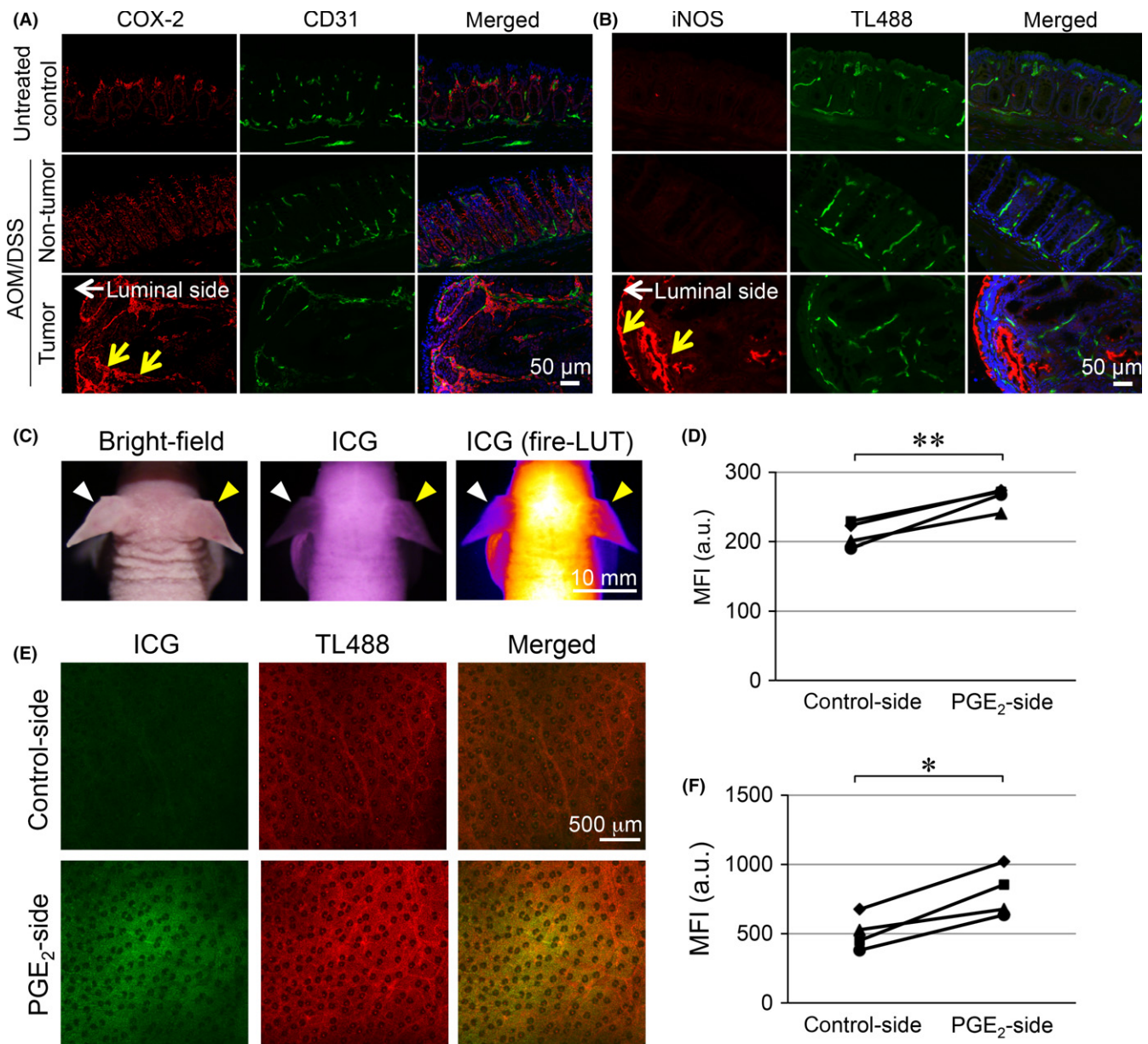


FIGURE 5 Immunofluorescence imaging of molecules related to vascular permeability in mouse colon tumor tissues and in vitro endothelial cell permeability assay. For immunofluorescence, colon tissues obtained from azoxymethane (AOM)/dextran sodium sulfate (DSS)-treated mice or untreated mice at 18–20 weeks after AOM initiation were used. (A) Immunofluorescence images of COX-2 (red) and CD31 (green) with nuclear staining (blue). White arrow indicates the direction of luminal side of tumor tissues. Yellow arrows indicate COX-2⁺ stromal cells. (B) Immunofluorescence images of inducible nitric oxide synthase (iNOS) (red) with blood vessel (*Lycopersicon esculentum* [tomato] lectin conjugated with DyLight [TL488], green) and nuclear (blue) staining. White arrow indicates the direction of luminal side of tumor tissues. Yellow arrows indicate iNOS⁺ tumor cells. (C) Representative wide-field images of indocyanine green (ICG) fluorescence 1 min after intradermal injection of vehicle (left ear; white arrowhead) or prostaglandin E₂ (PGE₂) (right ear; yellow arrowhead). ICG fluorescence was also shown by fire-lookup table (LUT). (D) Mean fluorescence intensity (MFI) in the wide-field images of ICG fluorescence (n = 4). **P < .01 (matched-pair t-test). (E) Representative high-power images of ICG fluorescence 10–12 min after intradermal injection of vehicle (left ear) or PGE₂ (right ear). (F) MFI in the high-power images of ICG fluorescence (n = 4). *P < .05 (matched-pair t-test)

(Figure 4B). The CD31⁺ area in normal colon tissues of AOM/DSS-treated mice did not differ from that of untreated mice (Figure 4B).

3.5 | Vascular permeability in colon tumor tissues

Vascular permeability is known to be promoted by inflammatory mediators, such as COX-2, iNOS, and HO-1.³³ Immunoreactivity of COX-2

was observed in stromal cells in the colon tissues (Figure 5A). The COX-2⁺ cells were distributed in the interstitium of lamina propria mucosa in normal colon tissues of untreated control mice or AOM/DSS-treated mice. In the colon tumor tissues, COX-2⁺ stromal cells were profoundly increased (Figure 5A). Immunoreactivity of HO-1 was also observed in stromal cells in the colon tissues (Figure S4). Although HO-1⁺ stromal cells in the tumor tissues were not abundant compared with COX-2⁺

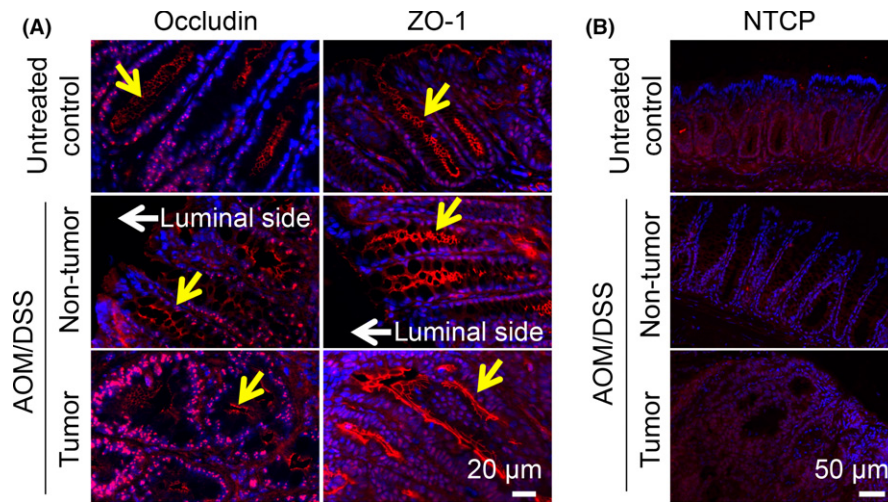


FIGURE 6 Immunofluorescence imaging of tight junction and transporter molecules in mouse colon tumor tissues. Immunofluorescence was carried out using colon tissue sections obtained from azoxymethane (AOM)/dextran sodium sulfate (DSS)-treated mice or untreated mice at 18–20 weeks after AOM initiation. (A) Immunofluorescence images of occludin or zonula occludens-1 (ZO-1) (red) with nuclear staining (blue). White arrow indicates the direction of luminal side of tumor tissues. Yellow arrows indicate occludin⁺ or ZO-1⁺ apical cell borders. (B) Immunofluorescence images of sodium-taurocholate co-transporting polypeptide (NTCP) (red) with nuclear staining (blue)

stromal cells, HO-1⁺ stromal cells were also increased in tumor tissues compared with normal colon tissues of untreated control mice or AOM/DSS-treated mice (Figure S4). Immunoreactivity of iNOS was also increased in tumor tissues, whereas it was rarely observed in normal colon tissues (Figure 5B). Most of the iNOS⁺ cells were found to be tumor cells at the tumor luminal surface. Endothelial cells did not express these inflammatory mediators (Figure 5A,B and Figure S4).

In the endothelial cell permeability assay using an HH cell monolayer (Document S1), ICG passed through the membrane without the monolayer, whereas ICG reduced permeability through the non-treated monolayer (Figure S5). Treatment with LPS to the monolayer weakly but insignificantly increased endothelial permeation of ICG (Figure S5). Endothelial permeation of ICG was also increased under PGE₂ or H₂O₂ treatment conditions, but the difference was statistically insignificant when compared with no treatment condition (Figure S5). In coculture experiments using a HUVEC monolayer with HT-29 cells and THP-1 cells (Document S1), endothelial permeation of ICG was weakly but insignificantly increased in the condition of HUVEC with HT-29 and THP-1 cells in combination, LPS-activated THP-1 cells alone and LPS-activated THP-1 cells and HT-29 cells in combination (Figure S5).

In the *in vivo* vascular permeability assay, ICG fluorescence was significantly increased in the ear after intradermal injection of PGE₂ compared with ears injected with PBS (Figure 5C–F).

3.6 | Expression of tight junction and transporter molecules in colon tumor tissues

The localization of occludin at the apical cell border was observed both in the tumor tissues of AOM/DSS-treated mice and normal colon epithelium of untreated control mice or AOM/DSS-treated mice, whereas immunoreactivity of occludin in the tumor cell cytoplasm was increased compared with the normal colon

epithelium (Figure 6A). Zonula occludens-1 was expressed at the apical cell border both in the normal tissues and tumor tissues. The immunoreactivity of zonula occludens-1 in the tumor cells was not changed from normal colon epithelium (Figure 6A). Immunoreactivity of NTCP was observed at the cell surface membrane both in the tumor cells and normal colon epithelial cells (Figure 6B). In the ICG enema experiment using AOM/DSS-treated mice, ICG did not accumulate in the tumor tissues (Figure S6).

4 | DISCUSSION

We have previously reported the utility of *i.v.* administered ICG in tumor detection using a mouse xenograft tumor model of a human colon cancer cell line.²⁴ Similar results were also obtained in metastatic lesions of clinical colorectal cancers, including their carcinomatosis,^{17,18} metastatic lymph node,¹⁹ or metastatic liver tumors using ICG.²⁰ However, there are no reports regarding the capability of ICG-based tumor imaging in colitis-associated colon cancer. The current animal model was created by 1 week of treatment with 5 w/v% DSS after AOM injection followed by a 4–20-week observation period. We further showed that ICG-based tumor imaging can be achieved in slowly growing colon tumors developed in animals treated with 1 week of 2 w/v% DSS after AOM injection with a 61-week observation period (Figure S7). Thus, the present study is the first report in which *i.v.* administered ICG was used in the identification of colon tumor lesions of an AOM/DSS-induced colitis-associated colon cancer model. Furthermore, ICG fluorescence signal in the current model showed correlation with tumor malignancy. Judging from the data of the receiver operating characteristic analysis, this technique can be applied to diagnosis of colitis-associated colon tumors.

Colon tumor tissues induced in the current animal model showed distorted and thick vasculature. Immunofluorescence microscopy analysis revealed that the CD31⁺ endothelial cell area in the tumor tissues was increased compared to the normal colon tissues. A previous study using several experimentally induced or spontaneously occurring tumors showing different angiogenesis capabilities reported that the fluorescence intensity of i.v. administered ICG correlates with microvascular density.²⁷ These results suggested that ICG accumulation in the tumor tissues was likely promoted by increasing tumor vascularity, leading to an increase in the chance for ICG to extravasate from tumor blood vessels.

In the present study, ICG fluorescence was distributed in the stromal tissues around the tumor blood vessels, whereas only weak ICG fluorescence was observed in the normal colon stromal tissues. Therefore, it can be postulated that blood vessel permeability of ICG plays a major role in ICG accumulation in the tumor tissues. It is known that extravasation of i.v. administered agents from blood vessels is promoted by the absence of pericytes.³⁴ However, in the present study, endothelial cells covered with/without α -smooth muscle actin-positive pericytes were observed in both normal colon tissues and colon tumor tissues. Therefore, these results suggest a minor role of the lack of pericyte coverage of endothelial cells in ICG-mediated tumor enhancement in the current model. However, vascular permeability is also known to be promoted by inflammatory mediators, such as COX-2, iNOS, and HO-1.³³ In our study, strong immunoreactivities of COX-2, iNOS, and HO-1 were observed in the AOM/DSS-induced tumor colon tissues, similar to previous studies.^{35,36} Furthermore, we showed that endothelial cell permeability of ICG in vitro was promoted by both PGE₂, a downstream product of COX-2,³³ and H₂O₂, an upstream reactive oxygen species of iNOS.^{33,37} Prostaglandin E₂ is known to increase local blood flow, resulting in vascular hyperpermeability.³² In the present study, intradermal injection of PGE₂ induced ICG permeability and accumulation in normal ear tissues, suggesting that enhanced permeability induced by PGE₂ was likely to be one of the mechanisms of tumor accumulation of ICG. Taken together, these results suggest that preferential accumulation of ICG in the tumor tissues can be attributed to the increase of tumor vascular permeability involving inflammatory mediators, such as COX-2 and iNOS, in conjunction with increasing tumor vasculature. In addition, accumulation capability of agents to the tumor tissues may be affected by impaired lymphatic drainage, which enhances agent retention in the tumor tissues, and enhanced vascular permeability, which promotes agent delivery to the tumor tissues.³⁸ Therefore, future work will be needed to clarify the contribution of the retention effect on ICG-based tumor imaging.

In the AOM/DSS-induced tumor tissues in the present study, tumor cells did not take up ICG, whereas ICG was distributed in the stromal tissues around the tumor parenchyma. Furthermore, ICG did not accumulate in the tumor tissues, even in the ICG enema experiment, in contrast to ICG accumulation by ICG enema in AOM-induced colon tumor tissues using rats in our previous study.²⁵ In our previous study using a mouse xenograft model of

human colon cancer cells, we revealed that cellular uptake of ICG is mediated by endocytosis in association with disruption of tight junctions.²⁴ In another study using rats, as mentioned above, we also reported altered expression of occludin, which could lead to disruption of tight junctions and further endocytosis of ICG, in parallel with tumor cellular uptake of ICG.²⁵ However, in the present study, immunolocalization of occludin in the tumor cells was observed at the apical cell border, similar to normal epithelial cells, suggesting the formation of functionally active tight junctions in tumor cells. These data suggest that tumor cells developed in the current model did not have ICG uptake capability because of low endocytic activity in conjunction with the formation of tight junctions.

In conclusion, our data indicated that fluorescence contrast-enhanced imaging following i.v. administered ICG can be applied to the detection of colon tumors in a mouse colitis-associated colon cancer model. The tumor tissue preference of ICG in the present model can be attributed to the enhanced vascular leakage of ICG in association with overexpression of inflammatory mediators, such as COX-2 and iNOS, in conjunction with increased tumor vascularity. Our findings provide the justification for the choice of ICG-based colon tumor imaging, irrespective of the tumor cell phenotype.

ACKNOWLEDGMENTS

The authors thank Shigeko Suzuki (Tokyo University of Agriculture and Technology) for her technical assistance in preparing the histological specimens.

CONFLICT OF INTEREST

N. Onda, S. Yamashita, M. Kojima, and S. Matsumoto are employees of Olympus Corporation. M. Shibutani received a research grant from Olympus Corporation. The other authors have no potential conflict of interest to disclose.

ORCID

Makoto Shibutani  <http://orcid.org/0000-0003-3417-9697>

REFERENCES

1. Grivennikov SI. Inflammation and colorectal cancer: colitis-associated neoplasia. *Semin Immunopathol.* 2013;35:229-244.
2. Hata K, Kishikawa J, Anzai H, et al. Surveillance colonoscopy for colitis-associated dysplasia and cancer in ulcerative colitis patients. *Dig Endosc.* 2016;28:260-265.
3. Shukla R, Salem M, Hou JK. Use and barriers to chromoendoscopy for dysplasia surveillance in inflammatory bowel disease. *World J Gastrointest Endosc.* 2017;9:359-367.
4. Mitsunaga M, Kosaka N, Choyke PL, et al. Fluorescence endoscopic detection of murine colitis-associated colon cancer by topically applied enzymatically rapid-activatable probe. *Gut.* 2013;62:1179-1186.

5. Atreya R, Goetz M. Molecular imaging in gastroenterology. *Nat Rev Gastroenterol Hepatol*. 2013;10:704-712.
6. Nguyen QT, Tsien RY. Fluorescence-guided surgery with live molecular navigation—a new cutting edge. *Nat Rev Cancer*. 2013;13:653-662.
7. Lee JH, Wang TD. Molecular endoscopy for targeted imaging in the digestive tract. *Lancet Gastroenterol Hepatol*. 2016;1:147-155.
8. Weissleder R, Pittet MJ. Imaging in the era of molecular oncology. *Nature*. 2008;452:580-589.
9. Kobayashi H, Ogawa M, Alford R, Choyke PL, Urano Y. New strategies for fluorescent probe design in medical diagnostic imaging. *Chem Rev*. 2010;110:2620-2640.
10. Alford R, Simpson HM, Duberman J, et al. Toxicity of organic fluorophores used in molecular imaging: literature review. *Mol Imaging*. 2009;8:341-354.
11. Gotoh K, Yamada T, Ishikawa O, et al. A novel image-guided surgery of hepatocellular carcinoma by indocyanine green fluorescence imaging navigation. *J Surg Oncol*. 2009;100:75-79.
12. Ishizawa T, Fukushima N, Shibahara J, et al. Real-time identification of liver cancers by using indocyanine green fluorescent imaging. *Cancer*. 2009;115:2491-2504.
13. Ntziachristos V, Yodh AG, Schnall M, et al. Concurrent MRI and diffuse optical tomography of breast after indocyanine green enhancement. *Proc Natl Acad Sci USA*. 2000;97:2767-2772.
14. Yokoyama J, Fujimaki M, Ohba S, et al. A feasibility study of NIR fluorescent image-guided surgery in head and neck cancer based on the assessment of optimum surgical time as revealed through dynamic imaging. *Onco Targets Ther*. 2013;6:325-330.
15. Okusanya OT, Holt D, Heitjan D, et al. Intraoperative near-infrared imaging can identify pulmonary nodules. *Ann Thorac Surg*. 2014;98:1223-1230.
16. Tummers QR, Hoogstins CE, Peters AA, et al. The value of intraoperative near-infrared fluorescence imaging based on enhanced permeability and retention of indocyanine green: feasibility and false-positives in ovarian cancer. *PLoS ONE*. 2015;10:e0129766.
17. Barabino G, Klein JP, Porcheron J, Grichine A, Coll JL, Cottier M. Intraoperative near-infrared fluorescence imaging using indocyanine green in colorectal carcinomatosis surgery: proof of concept. *Eur J Surg Oncol*. 2016;42:1931-1937.
18. Liberale G, Vankerckhove S, Caldon MG, et al. Fluorescence imaging after indocyanine green injection for detection of peritoneal metastases in patients undergoing cytoreductive surgery for peritoneal carcinomatosis from colorectal cancer: A pilot study. *Ann Surg*. 2016;264:1110-1115.
19. Liberale G, Galton MG, Moreau M, et al. Ex vivo detection of tumoral lymph nodes of colorectal origin with fluorescence imaging after intraoperative intravenous injection of indocyanine green. *J Surg Oncol*. 2016;114:348-353.
20. Boogerd LS, Handgraaf HJ, Lam HD, et al. Laparoscopic detection and resection of occult liver tumors of multiple cancer types using real-time near-infrared fluorescence guidance. *Surg Endosc*. 2017;31:952-961.
21. Ishizawa T, Masuda K, Urano Y, et al. Mechanistic background and clinical applications of indocyanine green fluorescence imaging of hepatocellular carcinoma. *Ann Surg Oncol*. 2014;21:440-448.
22. Shibasaki Y, Sakaguchi T, Hiraide T, et al. Expression of indocyanine green-related transporters in hepatocellular carcinoma. *J Surg Res*. 2015;193:567-576.
23. de Graaf W, Häusler S, Heger M, et al. Transporters involved in the hepatic uptake of ^{99m}Tc-mebrofenin and indocyanine green. *J Hepatol*. 2011;54:738-745.
24. Onda N, Kimura M, Yoshida T, Shibutani M. Preferential tumor cellular uptake and retention of indocyanine green for in vivo tumor imaging. *Int J Cancer*. 2016;139:673-682.
25. Onda N, Mizutani-Morita R, Yamashita S, et al. Fluorescence contrast-enhanced proliferative lesion imaging by enema administration of indocyanine green in a rat model of colon carcinogenesis. *Onco-target*. 2017;8:90278-90290.
26. Kosaka N, Mitsunaga M, Longmire MR, Choyke PL, Kobayashi H. Near infrared fluorescence-guided real-time endoscopic detection of peritoneal ovarian cancer nodules using intravenously injected indocyanine green. *Int J Cancer*. 2011;129:1671-1677.
27. Madajewski B, Judy BF, Mouchli A, et al. Intraoperative near-infrared imaging of surgical wounds after tumor resections can detect residual disease. *Clin Cancer Res*. 2012;18:5741-5751.
28. Suzuki R, Kohno H, Sugie S, Tanaka T. Dose-dependent promoting effect of dextran sodium sulfate on mouse colon carcinogenesis initiated with azoxymethane. *Histol Histopathol*. 2005;20:483-492.
29. Clapper ML, Cooper HS, Chang WC. Dextran sulfate sodium-induced colitis-associated neoplasia: a promising model for the development of chemopreventive interventions. *Acta Pharmacol Sin*. 2007;28:1450-1459.
30. Tanaka T. Development of an inflammation-associated colorectal cancer model and its application for research on carcinogenesis and chemoprevention. *Int J Inflamm*. 2012;2012:658786.
31. Kangawa Y, Yoshida T, Maruyama K, et al. Cilostazol and enzymatically modified isoquercitrin attenuate experimental colitis and colon cancer in mice by inhibiting cell proliferation and inflammation. *Food Chem Toxicol*. 2017;100:103-114.
32. Omori K, Kida T, Hori M, Ozaki H, Murata T. Multiple roles of the PGE₂-EP receptor signal in vascular permeability. *Br J Pharmacol*. 2014;171:4879-4889.
33. Maeda H. Vascular permeability in cancer and infection as related to macromolecular drug delivery, with emphasis on the EPR effect for tumor-selective drug targeting. *Proc Jpn Acad Ser B Phys Biol Sci*. 2012;88:53-71.
34. Kano MR, Komuta Y, Iwata C, et al. Comparison of the effects of the kinase inhibitors imatinib, sorafenib, and transforming growth factor- β receptor inhibitor on extravasation of nanoparticles from neovasculature. *Cancer Sci*. 2009;100:173-180.
35. Tanaka T, Kohno H, Suzuki R, Yamada Y, Sugie S, Mori H. A novel inflammation-related mouse colon carcinogenesis model induced by azoxymethane and dextran sodium sulfate. *Cancer Sci*. 2003;94:965-973.
36. Kim M, Miyamoto S, Yasui Y, Oyama T, Murakami A, Tanaka T. Zerumbone, a tropical ginger sesquiterpene, inhibits colon and lung carcinogenesis in mice. *Int J Cancer*. 2009;124:264-271.
37. Simoneau B, Houle F, Huot J. Regulation of endothelial permeability and transendothelial migration of cancer cells by tropomyosin-1 phosphorylation. *Vasc Cell*. 2012;4:18.
38. Maeda H, Nakamura H, Fang J. The EPR effect for macromolecular drug delivery to solid tumors: Improvement of tumor uptake, lowering of systemic toxicity, and distinct tumor imaging in vivo. *Adv Drug Deliv Rev*. 2013;65:71-79.

SUPPORTING INFORMATION

Additional Supporting Information may be found online in the supporting information tab for this article.

How to cite this article: Nagahara R, Onda N, Yamashita S, et al. Fluorescence tumor imaging by i.v. administered indocyanine green in a mouse model of colitis-associated colon cancer. *Cancer Sci*. 2018;109:1638-1647.

<https://doi.org/10.1111/cas.13564>